Dating Ore Deposit Using Garnet U–Pb Geochronology: Example from the Xinqiao Cu–S–Fe–Au Deposit, Eastern China

Yu Zhang [1,2], Yongjun Shao [2], Rongqing Zhang [3], Dengfeng Li [4], Zhongfa Liu [2] and Huayong Chen [1,*]

[1] Key Laboratory of Mineralogy and Metallogeny, Guangzhou Institute of Geochemistry,
    Chinese Academy of Sciences, Guangzhou 510640, China; zyu2009@csu.edu.cn
[2] Key Laboratory of Metallogenic Prediction of Nonferrous Metals and Geological Environment Monitor,
    Central South University, Ministry of Education, Changsha 410083, China; shaoyongjun@126.com (Y.S.);
    liuzhongfa_ok@126.com (Z.L.)
[3] State Key Laboratory for Mineral Deposits Research, School of Earth Sciences and Engineering,
    Nanjing University, Xianlin University Town, Nanjing 210023, China; zhangrq1986@gmail.com
[4] School of Marine Sciences, Sun Yat-sen University, Guangzhou 510006, China; lidf3@mail.sysu.edu.cn
* Correspondence: huayongchen@gig.ac.cn; Tel./Fax: +86-020-85292708

Abstract: The large Xinqiao Cu–S–Fe–Au deposit in the Tongling ore district, Eastern China, is characterized by a large-scale stratiform orebody, in which garnet is widely distributed as the main gangue mineral associated with mineralization. Xinqiao garnet can be divided into early (Grt1) and late (Grt2) generations based on extensive back-scattered electron (BSE) imaging observations. Laser ablation (LA)-ICP-MS trace element and U–Pb isotope composition analyses indicate that uranium occurs homogeneously within the Xinqiao garnet, and Grt1 and Grt2 have weighted average ^{207}Pb-corrected ^{206}Pb/^{238}U ages of 137.0 ± 7.8 Ma (Mean standard weighted deviation (MSWD) = 4.9) and 129.6 ± 7.1 Ma (MSWD = 1.6), respectively, similar to the zircon U–Pb age (139.6 ± 1.5 Ma) of the Jitou intrusion. These garnet U–Pb ages, combined with the low MnO content and various Y/Ho ratios, suggest that the Xinqiao garnet is likely to have a magmatic hydrothermal replacement origin associated with the Jitou stock. Based on previous studies of the Xinqiao deposit, we infer that the Xinqiao stratiform orebody may have formed from the Early Cretaceous magmatic hydrothermal fluids associated with the Jitou stock, and may have been generated by the Early Cretaceous tectono-thermal event in Eastern China.

Keywords: Garnet U–Pb geochronology; Xinqiao Cu–S–Fe–Au deposit; Middle–Lower Yangtze River Valley metallogenic belt; Eastern China

1. Introduction

Skarn deposits are an abundant ore type and represent a globally important source of Cu, Fe, Pb, Zn, W, Ag, and Au [1,2]. The direct and precise dating of skarn mineralization is commonly conducted by Re–Os of molybdenite [3,4], U–Pb of titanite [5,6], ^{40}Ar/^{39}Ar of micas [7] and K-feldspars [8,9], and Sm–Nd of calcite [10]. However, due to the lack of suitable datable minerals, direct dating of skarn-type mineralization is still locally unsuccessful.

Garnet is a common mineral in skarn systems [11], and its distinct oscillatory chemical zonation can track the fluid–rock interaction history and provide a continuous physicochemical record of the hydrothermal evolution [12–18]. Moreover, due to high Lu/Hf and Sm/Nd ratios, garnet can be directly dated by Lu–Hf and Sm–Nd dating [19]. However, the commonly low Lu and Hf contents in

garnet constrain the application of Lu–Hf dating [20]. Garnet Sm–Nd isochron dating is severely complicated because of variable Nd initial isotope ratios [21]. On the other hand, grandite (the most common garnet type in skarn systems) commonly contains variable U and Th coupled with insignificant common Pb [22–24], enabling direct U–Pb dating of garnet to be a new method which has been recently applied in some skarn deposits [22,25].

The Tongling ore district is located in the Middle–Lower Yangtze River Valley metallogenic belt along the northern margin of the Yangtze Craton in Eastern China (Figure 1; [26]). It is characterized by widespread Early Cretaceous granitoids and numerous skarn deposits [26]. However, the large-scale stratiform orebodies in the Xinqiao Cu–S–Fe–Au deposit and the Dongguashan Cu–Au deposit (Figure 2; [27]) in this region are thought to be obviously different from typical skarn deposits. Due to a lack of convincing mineralization age data, the genesis of these stratiform orebodies has been controversial over the past forty years, and the hypotheses focus on (1) Late Paleozoic submarine exhalative mineralization [28–31]; (2) Early Cretaceous magmatic hydrothermal mineralization [26,32–35]; and (3) Early Cretaceous magmatism overprinting on Late Paleozoic submarine exhalative processes [36–39]. Extensive skarn alteration in these stratiform orebodies powerfully supports the magmatic hydrothermal hypothesis [32]. However, previous studies have documented that garnet can form via not only magmatic hydrothermal replacement but also magmatism and submarine sedimentary exhalative processes [2,40–42]. The two-stage Xinqiao grandite (And_{100} to $And_{50}Gro_{46}$), which is suggested to have formed by magmatic hydrothermal replacement, was discovered based on their major and trace element geochemical characteristics [18]; however, no robust absolute age data support this hypothesis.
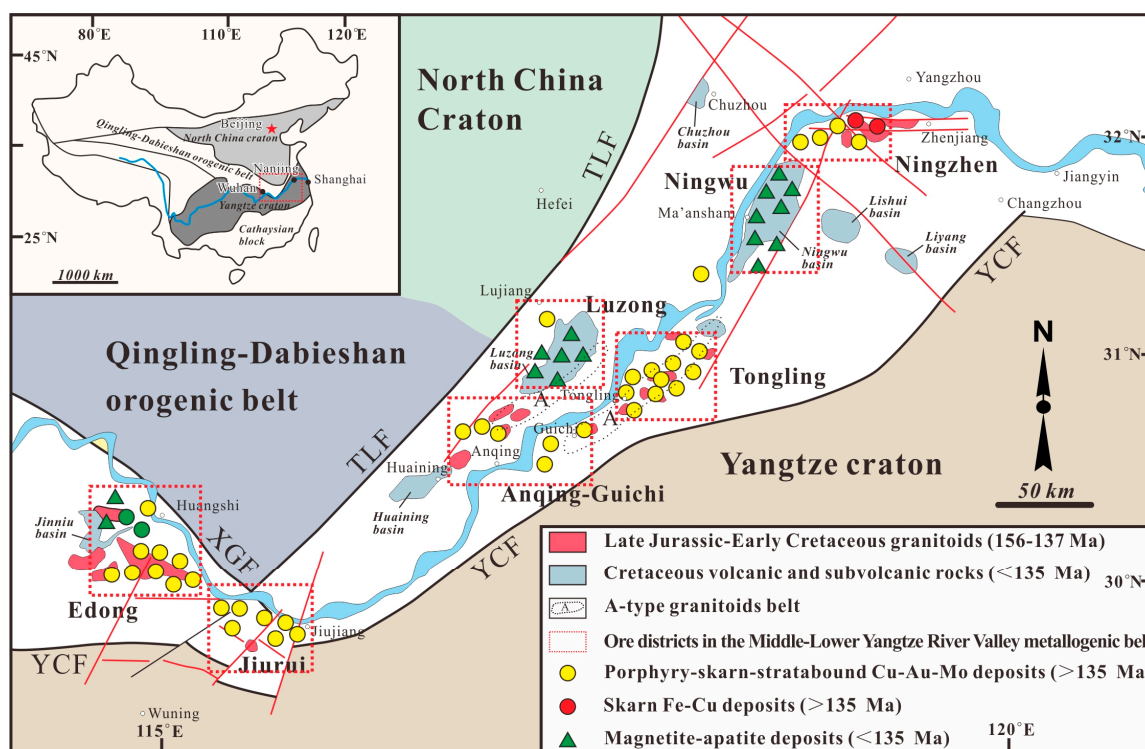

Figure 1. Location of the Tongling ore district in the Middle–Lower Yangtze River Valley metallogenic belt (after [26]). TLF: Tancheng–Lujiang fault; XGF: Xiangfan–Guangji fault; YCF: Yangxing–Changzhou fault.
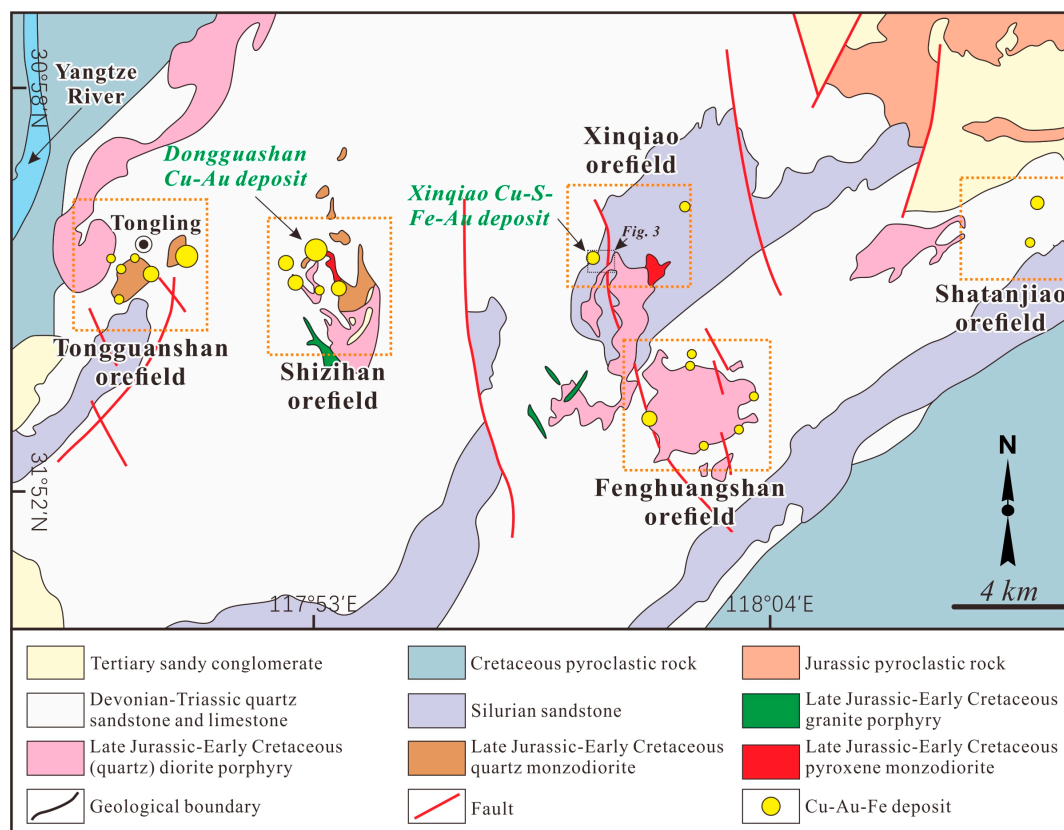
Figure 2. Geological map of the Tongling district (modified from [27]).

This study focuses on the garnet from the Xinqiao Cu–S–Fe–Au deposit (0.5 Mt Cu @ 0.71%, 75.5 Mt of sulfur @ 29.3%, 24.9 Mt Fe @ 46%, and 11.2 t Au @ 4.7 g/t; [43]) with the aim of constraining its mineralization age by using newly developed garnet U–Pb geochronology based on detailed field and mineralogical observations, discusses its implications on the Xinqiao ore genesis, and further introduces a new dating method for the skarn ore deposit type.

2. Geological Setting

2.1. Regional Geology

The Tongling ore district is the largest Cu–Au–Fe–Mo ore district in the Middle–Lower Yangtze River Valley metallogenic belt and hosts numerous skarn deposits associated with the Early Cretaceous tectono-thermal event (namely, widespread tectonics and magmatic activities generated from the subduction of the paleo-Pacific plate and the continental crust delamination of the Yangtze Craton) in Eastern China (Figures 1 and 2; [33,44]). More than 50 ore deposits have been discovered in the Tongling district, and are clustered in the Tongguanshan, Shizishan, Xinqiao, Fenghuangshan, and Shatanjiao orefields from east to west (Figure 2; [45]). Sedimentary rocks exposed in the area have ages spanning from the Silurian to the Cretaceous, excluding the Middle–Late Devonian, with dominant lithologies of sandy conglomerate, pyroclastic rocks, (quartz) sandstone, and limestone [27,46,47]. The Lower Permian and the Lower Triassic systems are dominated by limestone and are important ore-hosting rocks of the widespread skarn mineralization in this district. The unconformity between the Upper Devonian System and the Upper Carboniferous System hosts the economically significant stratiform mineralization in this district, such as the Xinqiao and Dongguashan deposits. Structurally, the region contains NE-trending folds and NNE- and NW-trending faults which controlled the emplacement of intrusions. More than 70 igneous intrusions are widely distributed in the region, and dominated by high-K calc-alkaline granite porphyry, (quartz) diorite porphyry, and quartz monzodiorite with ages from 156 ± 2 Ma (muscovite $^{40}Ar/^{39}Ar$ dating) to 137 ± 1 Ma (laser ablation (LA)-ICP-MS zircon U–Pb dating), occurring as composite stocks, dikes, and sills (Figure 2; [26,47–49]).

2.2. Ore Deposit Geology

The sedimentary rocks that crop out in the mining area range from Middle–Upper Silurian sandstone to Upper Triassic sandy conglomerate, whereas the Lower Carboniferous unit is absent. The NE-trending Dachengshan anticline and the NNE-trending Shenchong syncline are the major structures, and the junction of their hinges is an advantageous location of magmatic rocks and orebody (Figure 3a; [44]). The Jitou stock, as the dominant igneous rock, is a multiphase intrusion with quartz diorite at the center and diorite porphyry along the margin. The quartz diorite was dated to 139.6 ± 1.5 Ma by LA-ICP-MS zircon U–Pb geochronology [50]).
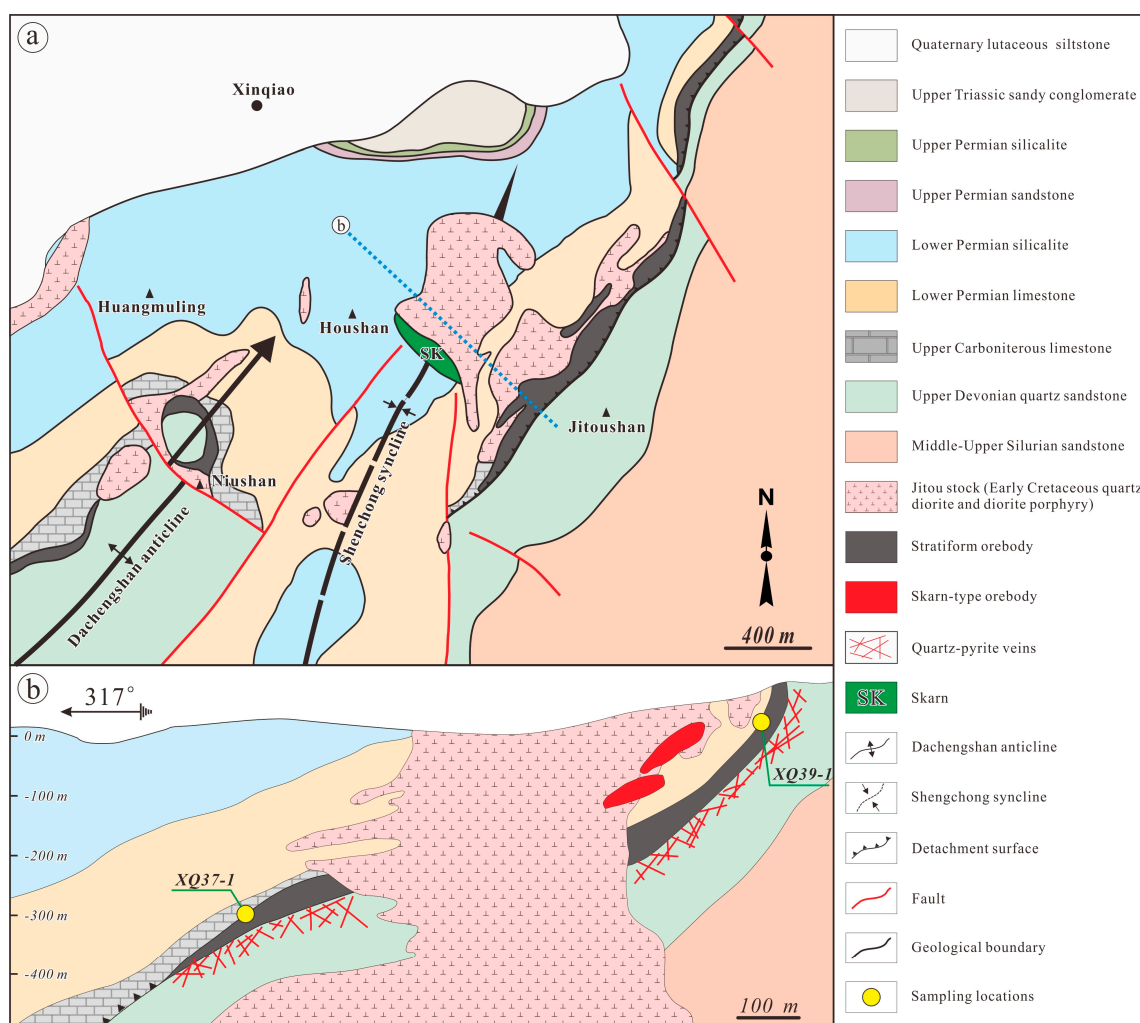

Figure 3. (**a**) Geological map and (**b**) representative cross section of the Xinqiao Cu–S–Fe–Au deposit (after [44,51], respectively).

The major mineralization type is the economically significant stratiform mineralization (accounting for 90% of the Cu, S, and Fe reserves) which is confined along the unconformity between the Upper Devonian quartz sandstone and the Upper Carboniferous limestone (Figure 3b; [51]). The major stratiform orebody is NW-dipping and has length and width of 2560 m and 1810 m, respectively, with an average thickness of 21 m (Figure 3b; [51]). In the footwall of the stratiform orebody, the quartz–pyrite stockwork occurs in the Upper Devonian quartz sandstone. Field geologic and petrographic observations indicate that ore minerals in the stratiform orebody include magnetite, chalcopyrite, pyrite, pyrrhotite, and hematite, whereas gangue minerals include primarily garnet, diopside, wollastonite, epidote, chlorite, quartz, and calcite. Detailed field investigation indicates that the wallrock alteration products of the hanging wall of the stratiform orebody include garnet, sericite, quartz, chlorite, and kaolinite, with silicic alteration developed in the footwall of the orebody [18,35,50,52]. Based on mineral assemblages and textural relationships, the Xinqiao mineralization

was divided into five stages [18,35], namely, early skarn (Stage I, dominated by garnet and diopside), late skarn (Stage II, featured by abundant epidote), metallic oxide (Stage III, dominated by hematite and magnetite), colloform pyrite (Stage IV, dominated by colloform pyrite) and quartz–sulfide (Stage V, featuring abundant quartz, chalcopyrite, pyrite, and gold occurring as Au nanoparticles in pyrite).

3. Sample Descriptions

Two garnet skarn samples were collected from the hanging wall of the stratiform orebody in the southwest part of the 13 m platform at the Xinqiao open pit (XQ39-1; Figure 4a) and W401 stope at −300 m depth (XQ37-1; Figure 4b). The garnet in sample XQ39-1 is beige to dark green in color, coexisting with coarse-grained wollastonite and crosscut by late-stage quartz veins (Figure 4a). Sample XQ37-1 is dominated by beige garnet coexisting with trace pyroxene and wollastonite (Figure 4b). The skarn minerals in Sample XQ37-1 are locally replaced by late irregular quartz and calcite (Figure 4b). Under the microscope, the garnet grains are typically subhedral or anhedral granular, homogenous, and contain no distinct oscillatory zoning (Figures 4c,d). The late quartz and calcite occur among garnet, pyroxene, and wollastonite particles, and pervasively replace these minerals (Figures 4c,d). In addition to quartz and calcite, late epidote also strongly replaces garnet, pyroxene, and wollastonite (Figures 4e–g), and occurs locally as pseudomorphs of garnet (Figure 4e).
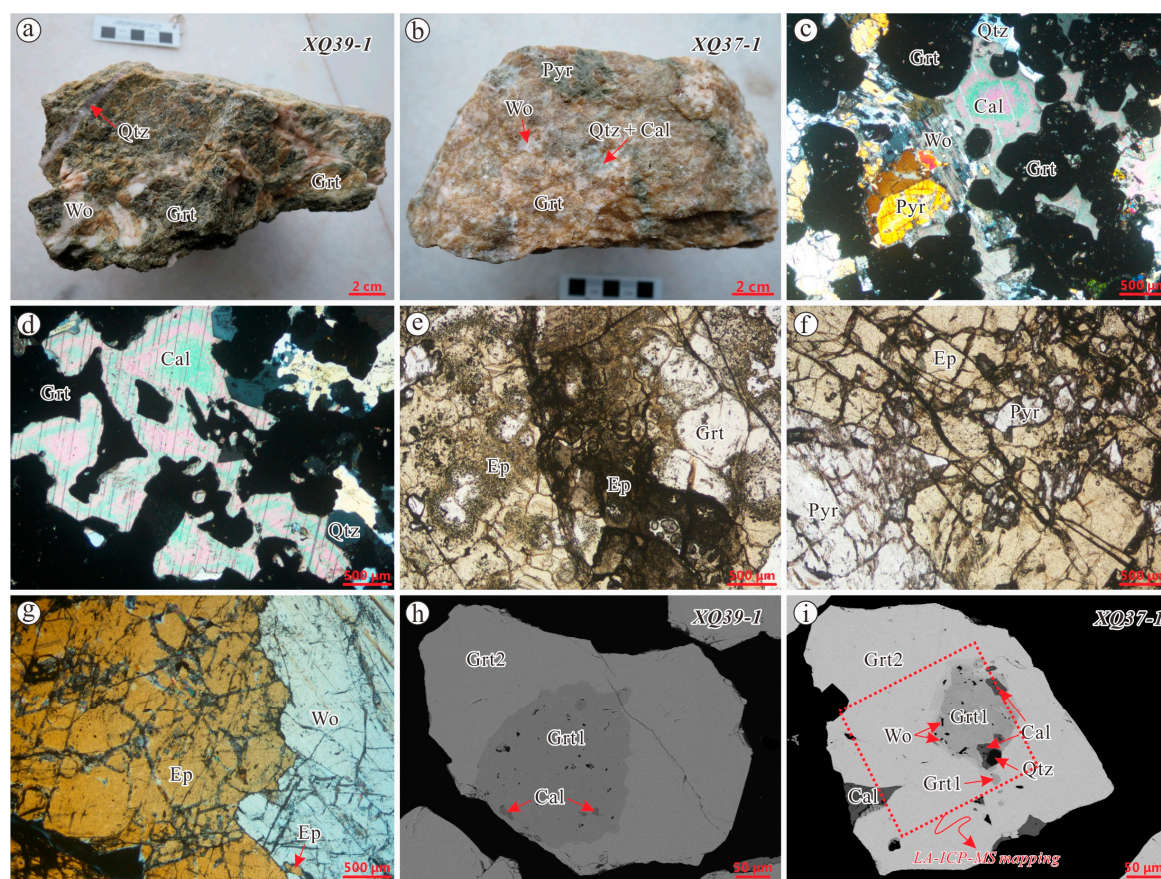

Figure 4. Photographs showing representative mineral assemblages and textural features of the garnet skarns. (**a**) Hand specimen for Sample XQ39-1, showing the skarn mineral assemblage of garnet–wollastonite, crosscut by late quartz vein. Garnet in sample XQ39-1 is from beige to dark green in color; (**b**) Hand specimen for Sample XQ37-1, showing the skarn mineral assemblage of garnet–wollastonite–pyroxene, locally replaced by late quartz and calcite; (**c**) The garnets are homogeneous and contain no distinct oscillatory zoning, coexisting with wollastonite and pyroxene and replaced by late calcite and quartz (CPL; XQ37-1); (**d**) Late quartz and calcite replace garnet (CPL; XQ37-1); (**e**) Late epidote extensively replaces garnet, and occur locally as a pseudomorph of garnet (PPL; XQ39-1); (**f**) Late epidote strongly replaces pyroxene (PPL; XQ39-1); (**g**) Late epidote strongly replaces wollastonite (PPL; XQ37-1); (**h**) Back-scattered electron (BSE) observation reveals two generations of

garnet, with no obvious chemical oscillatory zoning; (**i**) BSE observation reveals that Grt1 coexists with irregular wollastonite and is locally resorbed by late irregular calcite and quartz. Abbreviations: Qtz = Quartz; Wo = Wollastonite; Grt = Garnet; Pyr = Pyroxene; Cal = Calcite; Ep = Epidote; Grt1 = The early generation of garnet; Grt2 = The late generation of garnet.

Two types of garnet with different shades of gray (abundant dark gray Grt1 and local gray Grt2) were identified in samples XQ39-1 and XQ37-1 based on back-scattered electron (BSE) imaging observation. Neither have obvious chemical oscillatory zoning in BSE imaging (Figures 4h,i). Grt1 is anhedral granular and always occurs in the core of individual garnet grains (Figures 4h,i). It is locally resorbed by late irregular calcite and quartz (Figures 4h,i). Grt2 is anhedral granular, occurs around Grt1 (Figures 4h,i) and is locally resorbed by late irregular calcite (Figure 4i). Importantly, the contact boundary between Grt1 and Grt2 is irregular (Figure 4h), indicating replacement texture, rather than growth zoning. These two garnets, therefore, correspond to two different generations, i.e., the early generation (Grt1) and the late generation (Grt2), rather than the growth zoning of garnet normally documented in other studies [11,53].

4. Analytical Methods

Laser mount preparation and petrographic microscopy were conducted at the Key Laboratory of Mineralogy and Metallogeny, Guangzhou Institute of Geochemistry, Chinese Academy of Sciences, Guangzhou, China. Prior to LA-ICP-MS trace element and U–Pb isotope analysis, Electron Probe Microanalyzer (EPMA) analysis, mainly including in situ major element analysis and back-scattered electron (BSE) observation, was carried out in the School of Geosciences and Info-Physics of the Central South University, using a 1720 EPMA (Shimadzu Corporation, Tokyo, Japan). Analytical parameters were 15 Kv (acc. voltage), 2.0×10^{-8} A (probe current), and 1 μm (spot size), Natural quartz was used as the standard to correct the SiO_2 concentration in garnet. Detection limits for the elements are below 0.01 wt %. Data were corrected using the internal ZAF (Z = Atomic number, A = Absorption and F = Fluorescence) correction program.

Subsequently, garnet U–Pb dating, trace element analysis, and mapping were performed using laser ablation inductively coupled plasma mass spectrometry (LA-ICP-MS) at the Key Laboratory of Marine Resources and Coastal Engineering, Sun Yat-sen University (Guangzhou, China). The areas selected for U–Pb dating and trace element analysis were free of inclusions and fractures and approximate to EPMA analysis points. Laser ablation for garnet was performed using an ArF excimer laser ablation system (GeoLasPro; Microlas, Gottingen, Germany), and ion signal intensities were acquired using an Agilent 7700 × ICP-MS (Agilent, Santa Clara, CA, USA). A 44 μm spot was used with an energy density of 5 J/cm^2 and a repetition rate of 5 Hz. The trace element compositions of the garnet were calibrated against the National Institute of Standards and Technology Standard Reference Material 610, using the Si (Table 1) determined by electron microprobe as the internal standard. Zircon 91500 was used as the external standard to correct U–Pb isotopic ratios. Time-dependent drifts of U–Th–Pb isotopic ratios were corrected using a linear interpolation (with time) for every 10 analyses, based on the variations of Zircon 91500. The final uncertainties were propagated from uncertainties of the preferred and measured Zircon 91500 values, and from the measured sample values [54]. Garnet QC04 was used as the secondary standard for monitoring the precision and accuracy of the U–Pb dating results. The obtained mean $^{206}Pb/^{238}U$ age for QC04 is 131 ± 2 Ma (2σ; MSWD = 0.86; n = 10), which is consistent with the recommended values (130 ± 2 Ma, [22]). Each analysis consisted of 20 s of background measurement (laser-off) followed by 45 s of data acquisition. Data reduction was performed using ICPMSDataCal software [54]. Meanwhile, ISOPLOT 3.0 software [55] was used to construct the Tera–Wasserburg diagram and weighted mean calculations.

Table 1. Laser ablation (LA)-ICP-MS trace elements data (ppm) of the Xinqiao garnets.

No.	Sample	Type	SiO$_2$ (wt %)	Y	La	Ce	Pr	Nd	Sm	Eu	Gd	Tb	Dy	Ho	Er	Tm	Yb	Lu	U
1	XQ37-1	Grt1	38.38	110.56	1.07	6.34	2.02	15.60	7.12	1.98	9.62	1.71	11.21	2.68	7.55	1.05	8.16	1.13	2.83
2	XQ37-1	Grt1	38.58	78.84	1.92	7.18	2.40	17.52	5.67	1.55	7.27	1.22	7.84	1.82	5.21	0.76	5.62	0.85	3.84
3	XQ37-1	Grt1	37.56	73.37	0.49	2.41	2.77	18.46	2.01	0.69	4.09	0.89	6.67	1.65	5.04	0.67	5.82	0.76	3.42
4	XQ37-1	Grt1	39.11	80.31	1.33	8.28	2.73	18.97	5.48	1.57	7.21	1.17	8.36	1.78	5.57	0.77	6.32	0.90	2.92
5	XQ37-1	Grt1	37.80	71.85	0.50	2.76	2.88	16.38	2.39	0.69	4.77	0.87	6.55	1.60	5.04	0.74	5.53	0.71	3.51
6	XQ37-1	Grt1	38.59	69.72	0.55	2.47	2.90	17.17	2.16	0.74	4.00	0.79	6.17	1.46	4.71	0.71	5.13	0.75	3.59
7	XQ37-1	Grt1	36.81	74.62	0.58	2.62	2.85	20.28	2.52	0.71	4.52	0.97	6.68	1.72	5.76	0.75	6.06	0.75	3.64
8	XQ37-1	Grt1	37.86	68.43	0.52	2.44	2.66	17.34	2.10	0.63	4.16	0.82	6.53	1.54	4.70	0.78	5.80	0.71	4.23
9	XQ37-1	Grt1	36.86	72.40	0.98	3.26	3.38	20.67	1.74	0.65	3.93	0.90	6.70	1.61	4.80	0.71	5.53	0.78	4.57
10	XQ37-1	Grt1	37.95	68.89	0.54	2.43	2.76	17.89	1.77	0.58	3.95	0.80	5.98	1.53	4.79	0.67	5.48	0.69	4.20
11	XQ37-1	Grt1	38.97	50.15	1.50	10.32	3.68	28.73	8.64	2.00	8.05	1.03	5.83	1.16	3.19	0.44	3.01	0.38	5.35
12	XQ37-1	Grt1	38.63	57.99	2.66	10.05	3.29	19.31	5.82	1.56	6.84	0.91	6.64	1.46	4.12	0.51	3.83	0.52	5.23
13	XQ37-1	Grt1	35.91	70.27	0.47	2.32	2.79	22.34	1.96	0.72	4.17	0.89	6.55	1.61	5.08	0.78	6.11	0.75	3.91
14	XQ37-1	Grt1	38.77	72.28	0.68	3.08	2.91	22.09	2.49	0.77	4.49	1.04	6.73	1.64	4.93	0.80	5.13	0.74	3.63
15	XQ37-1	Grt1	37.98	38.07	2.52	13.61	3.58	21.32	5.39	1.13	5.06	0.64	4.24	0.95	2.49	0.34	2.37	0.36	4.43
16	XQ37-1	Grt1	38.07	70.82	0.83	4.93	3.41	22.92	2.58	0.88	4.51	0.86	6.42	1.59	4.82	0.71	5.69	0.75	5.31
17	XQ37-1	Grt1	37.78	44.06	2.25	15.28	4.31	28.16	7.06	1.33	7.13	0.93	5.46	1.13	2.91	0.34	2.75	0.41	6.85
18	XQ37-1	Grt1	38.49	96.25	1.96	15.41	4.88	30.23	8.42	2.65	9.08	1.52	9.74	2.32	6.56	0.97	6.68	1.03	7.65
19	XQ37-1	Grt1	38.37	104.11	1.91	11.04	3.03	20.75	7.23	1.89	9.42	1.51	10.40	2.31	7.09	1.02	7.61	0.93	5.49
20	XQ37-1	Grt1	37.96	282.27	1.48	10.00	3.22	25.82	14.89	4.37	23.38	4.29	30.50	7.32	21.04	3.23	22.85	3.17	6.26
21	XQ37-1	Grt1	39.60	39.04	2.63	15.71	5.87	30.30	3.92	1.26	3.84	0.62	4.00	0.87	2.51	0.37	2.76	0.40	13.93
22	XQ37-1	Grt1	39.91	63.47	2.14	14.47	4.21	27.06	6.04	1.72	6.26	0.86	5.79	1.57	4.11	0.61	3.76	0.63	10.08
23	XQ37-1	Grt1	37.75	62.74	0.82	4.91	3.37	21.32	2.49	0.80	4.00	0.75	5.78	1.39	4.33	0.62	4.91	0.67	5.20
24	XQ37-1	Grt1	38.09	57.05	1.28	5.40	3.46	19.99	3.16	0.92	3.95	0.71	5.46	1.28	3.74	0.53	4.26	0.61	5.22
25	XQ39-1	Grt1	39.38	68.77	1.56	5.98	3.37	27.90	2.53	0.83	4.05	0.80	6.24	1.50	4.84	0.75	5.20	0.71	6.88
26	XQ39-1	Grt1	36.99	97.96	2.16	11.98	3.84	23.41	6.30	1.87	9.19	1.57	10.49	2.36	6.67	0.97	6.96	0.95	5.52
27	XQ39-1	Grt1	39.09	66.43	2.53	15.14	4.39	25.09	6.42	1.68	7.21	1.08	7.13	1.58	4.57	0.63	4.66	0.70	5.56
28	XQ39-1	Grt1	38.61	141.16	1.21	7.63	2.92	20.85	8.35	2.41	12.03	1.92	14.81	3.41	10.88	1.58	12.17	1.62	4.91
29	XQ39-1	Grt1	39.36	125.33	1.68	6.10	2.30	18.17	7.46	1.96	12.36	1.91	13.42	3.09	8.39	1.16	9.25	1.28	2.57
30	XQ39-1	Grt1	38.98	94.80	1.22	8.37	2.90	19.64	5.99	1.68	7.67	1.42	9.62	2.10	6.48	0.96	7.07	0.97	3.56
31	XQ39-1	Grt1	38.66	58.77	1.23	9.04	2.84	19.99	5.50	1.43	6.30	1.03	6.38	1.36	4.00	0.54	4.04	0.58	3.34
32	XQ39-1	Grt1	37.88	296.84	1.59	10.55	3.30	27.47	14.89	4.73	25.61	4.51	32.37	8.04	22.67	3.29	23.49	3.33	6.85
33	XQ39-1	Grt1	39.91	127.47	0.92	4.02	1.69	13.67	6.56	2.30	9.23	1.86	13.81	3.04	8.31	1.31	9.25	1.18	1.69
34	XQ39-1	Grt1	38.88	230.21	1.39	8.91	2.94	25.47	10.11	3.24	15.73	3.44	24.17	6.14	17.65	2.71	19.48	2.53	4.69
35	XQ39-1	Grt1	39.36	121.33	0.65	4.53	1.79	13.33	6.52	2.38	11.37	1.91	12.49	2.80	8.24	1.14	8.34	1.21	1.60

36	XQ39-1	Grt1	38.03	73.35	1.33	10.37	3.53	20.58	6.52	1.59	6.59	1.13	7.33	1.64	4.98	0.70	5.26	0.72	4.89
37	XQ39-1	Grt1	39.12	63.74	1.63	9.54	2.94	19.32	5.47	1.64	5.81	0.94	6.45	1.45	4.20	0.62	4.45	0.61	5.89
38	XQ37-1	Grt2	35.59	3.28	12.52	77.87	13.09	34.21	2.85	4.09	0.93	0.14	0.46	0.09	0.16	0.03	0.23	0.03	11.20
39	XQ37-1	Grt2	35.28	17.93	9.99	68.33	11.90	34.02	2.66	4.25	2.00	0.30	2.04	0.40	1.28	0.16	1.22	0.13	10.91
40	XQ37-1	Grt2	36.37	5.40	9.75	69.80	9.17	23.25	2.13	2.15	1.08	0.13	0.67	0.09	0.24	0.03	0.19	0.04	10.15
41	XQ37-1	Grt2	35.90	13.96	4.90	30.51	3.95	10.57	1.96	1.18	2.36	0.32	1.73	0.32	0.89	0.11	0.81	0.10	3.58
42	XQ37-1	Grt2	36.76	11.97	5.85	38.31	5.52	16.36	2.38	1.68	2.35	0.29	1.60	0.27	0.67	0.11	0.61	0.10	4.46
43	XQ37-1	Grt2	36.32	18.00	5.02	33.60	4.68	14.41	3.64	1.45	3.56	0.46	2.42	0.45	0.96	0.13	0.91	0.11	4.91
44	XQ37-1	Grt2	36.41	10.72	7.36	44.06	7.09	26.42	2.55	3.05	2.45	0.25	1.53	0.26	0.53	0.08	0.86	0.07	7.51
45	XQ37-1	Grt2	35.36	11.19	6.36	47.82	7.28	21.77	2.48	2.69	2.60	0.29	1.36	0.29	0.71	0.07	0.70	0.07	7.15
46	XQ37-1	Grt2	35.65	11.75	14.09	65.80	8.82	23.06	2.33	2.50	2.04	0.22	1.45	0.26	0.75	0.08	0.63	0.08	10.37
47	XQ37-1	Grt2	36.37	11.42	7.32	45.10	6.03	16.50	1.88	1.63	2.35	0.26	1.59	0.25	0.71	0.08	0.69	0.08	6.59
48	XQ37-1	Grt2	35.23	16.90	5.29	55.04	8.61	21.59	1.72	2.49	2.49	0.36	2.37	0.40	1.04	0.10	1.14	0.13	6.73
49	XQ37-1	Grt2	35.89	4.28	11.21	70.60	10.63	28.63	1.76	2.66	1.27	0.14	0.58	0.10	0.25	0.03	0.19	0.03	9.40
50	XQ37-1	Grt2	34.92	18.19	7.22	59.64	9.46	27.36	3.00	3.09	2.55	0.43	2.24	0.48	1.26	0.15	1.12	0.13	8.26
51	XQ37-1	Grt2	36.72	4.99	12.60	77.15	12.85	34.11	2.70	4.03	1.41	0.18	0.41	0.11	0.33	0.04	0.15	0.04	12.90
52	XQ39-1	Grt2	38.04	4.71	10.46	66.53	9.86	27.51	1.77	2.37	1.51	0.14	0.65	0.12	0.31	0.04	0.28	0.04	9.11
53	XQ39-1	Grt2	35.78	4.10	10.00	64.68	9.37	25.78	1.98	1.90	1.97	0.17	0.50	0.13	0.18	0.02	0.18	0.02	9.69
54	XQ39-1	Grt2	34.63	17.68	4.94	46.82	7.39	24.14	3.27	2.60	2.73	0.33	1.85	0.35	0.92	0.15	0.93	0.13	5.80
55	XQ39-1	Grt2	34.95	16.17	8.23	67.02	9.48	23.31	2.84	2.52	2.53	0.29	1.74	0.38	0.85	0.10	0.86	0.13	8.33
56	XQ39-1	Grt2	36.14	2.93	10.73	65.37	9.61	22.68	1.03	1.96	0.67	0.10	0.36	0.06	0.17	0.03	0.12	0.02	8.86
57	XQ39-1	Grt2	36.16	4.93	16.90	94.77	12.75	30.36	1.89	2.30	1.43	0.13	0.64	0.11	0.26	0.04	0.24	0.03	15.43
58	XQ39-1	Grt2	35.29	18.16	5.95	46.87	7.41	21.02	2.67	2.28	3.32	0.42	2.00	0.43	1.11	0.15	1.08	0.14	5.97
59	XQ39-1	Grt2	35.46	3.66	11.81	73.06	10.57	26.64	1.78	2.24	0.92	0.10	0.45	0.07	0.21	0.03	0.22	0.03	10.54
60	XQ39-1	Grt2	35.70	12.29	5.67	36.16	5.25	16.52	2.84	1.33	2.67	0.36	1.45	0.26	0.58	0.07	0.56	0.07	5.86
61	XQ39-1	Grt2	36.41	3.83	11.91	73.07	11.19	33.07	1.65	2.89	0.92	0.10	0.52	0.08	0.16	0.03	0.17	0.03	10.19
62	XQ39-1	Grt2	37.85	7.51	12.67	75.12	11.62	33.95	2.16	3.25	2.10	0.20	0.88	0.17	0.40	0.06	0.41	0.06	11.84
63	XQ39-1	Grt2	36.15	21.87	4.59	30.36	5.07	14.85	2.50	2.01	3.01	0.45	2.68	0.56	1.32	0.20	1.26	0.12	5.00
64	XQ39-1	Grt2	35.17	6.32	11.04	68.67	9.86	27.32	1.81	2.26	1.24	0.13	0.77	0.12	0.42	0.05	0.32	0.06	9.18
65	XQ39-1	Grt2	36.32	3.07	10.99	70.11	9.82	26.77	1.57	2.23	0.99	0.10	0.51	0.07	0.19	0.02	0.18	0.02	9.52
66	XQ39-1	Grt2	35.75	4.37	11.13	71.26	10.20	27.43	1.58	2.32	1.02	0.12	0.63	0.09	0.23	0.03	0.22	0.03	10.28
67	XQ39-1	Grt2	35.64	7.95	10.62	74.38	10.29	26.22	2.83	2.49	2.18	0.19	1.26	0.22	0.52	0.08	0.57	0.09	10.97
68	XQ39-1	Grt2	35.50	4.51	11.60	71.88	10.24	28.77	1.83	2.28	1.05	0.09	0.42	0.10	0.29	0.04	0.24	0.04	11.39
69	XQ39-1	Grt2	36.99	4.15	12.65	79.89	11.47	30.15	1.82	2.48	1.75	0.13	0.62	0.10	0.23	0.03	0.24	0.03	11.94
70	XQ39-1	Grt2	35.84	9.58	9.54	67.59	9.95	25.59	2.44	2.34	2.03	0.20	1.07	0.20	0.55	0.06	0.47	0.06	9.69
71	XQ39-1	Grt2	35.51	4.33	12.82	80.63	11.09	28.26	1.86	2.21	1.22	0.12	0.56	0.10	0.22	0.03	0.25	0.03	12.68
72	XQ39-1	Grt2	35.77	14.54	9.86	74.29	10.27	25.05	2.74	2.65	2.39	0.32	1.81	0.36	0.88	0.11	0.86	0.13	10.45
73	XQ39-1	Grt2	36.02	3.18	13.09	82.29	11.68	29.66	1.56	2.20	0.92	0.08	0.42	0.06	0.17	0.03	0.19	0.03	13.18

74	XQ39-1	Grt2	35.07	17.85	5.19	49.49	8.82	26.68	3.17	3.13	2.17	0.36	1.92	0.41	0.80	0.11	1.17	0.13	6.13
75	XQ39-1	Grt2	35.68	3.06	12.12	73.29	10.44	27.00	1.69	2.15	0.95	0.08	0.59	0.06	0.21	0.03	0.14	0.02	10.91
76	XQ39-1	Grt2	35.68	2.97	15.86	85.42	11.06	28.76	2.06	1.72	0.96	0.10	0.49	0.07	0.15	0.02	0.21	0.02	14.27
77	XQ39-1	Grt2	36.11	4.26	12.19	74.08	10.32	29.23	1.56	2.27	0.79	0.08	0.32	0.08	0.19	0.05	0.29	0.04	12.33
78	XQ39-1	Grt2	35.52	20.17	4.85	45.31	7.55	22.32	3.67	2.68	3.17	0.44	2.57	0.45	1.20	0.13	1.22	0.17	5.71
79	XQ39-1	Grt2	35.51	13.70	11.57	62.85	9.25	27.66	2.32	3.06	1.93	0.29	1.59	0.31	0.85	0.11	0.89	0.10	8.66
80	XQ39-1	Grt2	35.44	2.57	18.31	100.04	13.21	33.45	1.68	2.26	0.83	0.08	0.32	0.05	0.14	0.02	0.15	0.02	17.34
81	XQ39-1	Grt2	35.63	2.99	13.44	80.82	12.29	35.29	1.77	3.18	0.90	0.10	0.38	0.06	0.17	0.02	0.36	0.02	11.61
82	XQ39-1	Grt2	35.66	16.03	5.80	53.15	7.84	22.85	2.75	2.57	2.79	0.38	1.91	0.35	0.99	0.12	0.59	0.13	6.35
83	XQ39-1	Grt2	36.25	7.71	14.64	72.85	10.17	25.13	2.21	2.83	1.77	0.19	0.99	0.17	0.39	0.06	0.44	0.06	11.15
84	XQ39-1	Grt2	35.49	2.40	20.34	108.44	14.07	33.63	1.74	2.42	0.79	0.06	0.30	0.05	0.15	0.02	0.16	0.02	17.81
85	XQ39-1	Grt2	35.58	3.85	10.77	67.76	10.23	30.23	1.93	2.61	1.10	0.12	0.49	0.08	0.21	0.02	0.17	0.02	8.91
86	XQ39-1	Grt2	34.96	17.72	7.12	60.99	9.98	26.52	2.57	3.35	2.94	0.37	2.34	0.35	1.17	0.11	0.78	0.08	8.24

5. Results

5.1. Trace Element Geochemistry

A total of 86 spot analyses for LA-ICP-MS trace element compositions were conducted on XQ37-1 and XQ39-1, including 37 spots in Grt1 grains and 49 spots in Grt2 grains. Trace element concentrations of the garnets are shown in Table 1. Grt1 and Grt2 have U contents ranging from 1.60 to 13.93 ppm (average: 4.95 ppm) and 3.58 to 17.81 ppm (average: 9.58 ppm). LA-ICP-MS trace element mapping data (Figure 5) reveal that the contents of Al, Fe, Y, and rare-earth elements are homogeneous within a specific garnet generation. Grt1 has higher concentrations of Al, Y, and rare-earth elements (except for La) than Grt2. Uranium is relatively homogeneous and enriched within Grt1, but is heterogeneously distributed in Grt2.
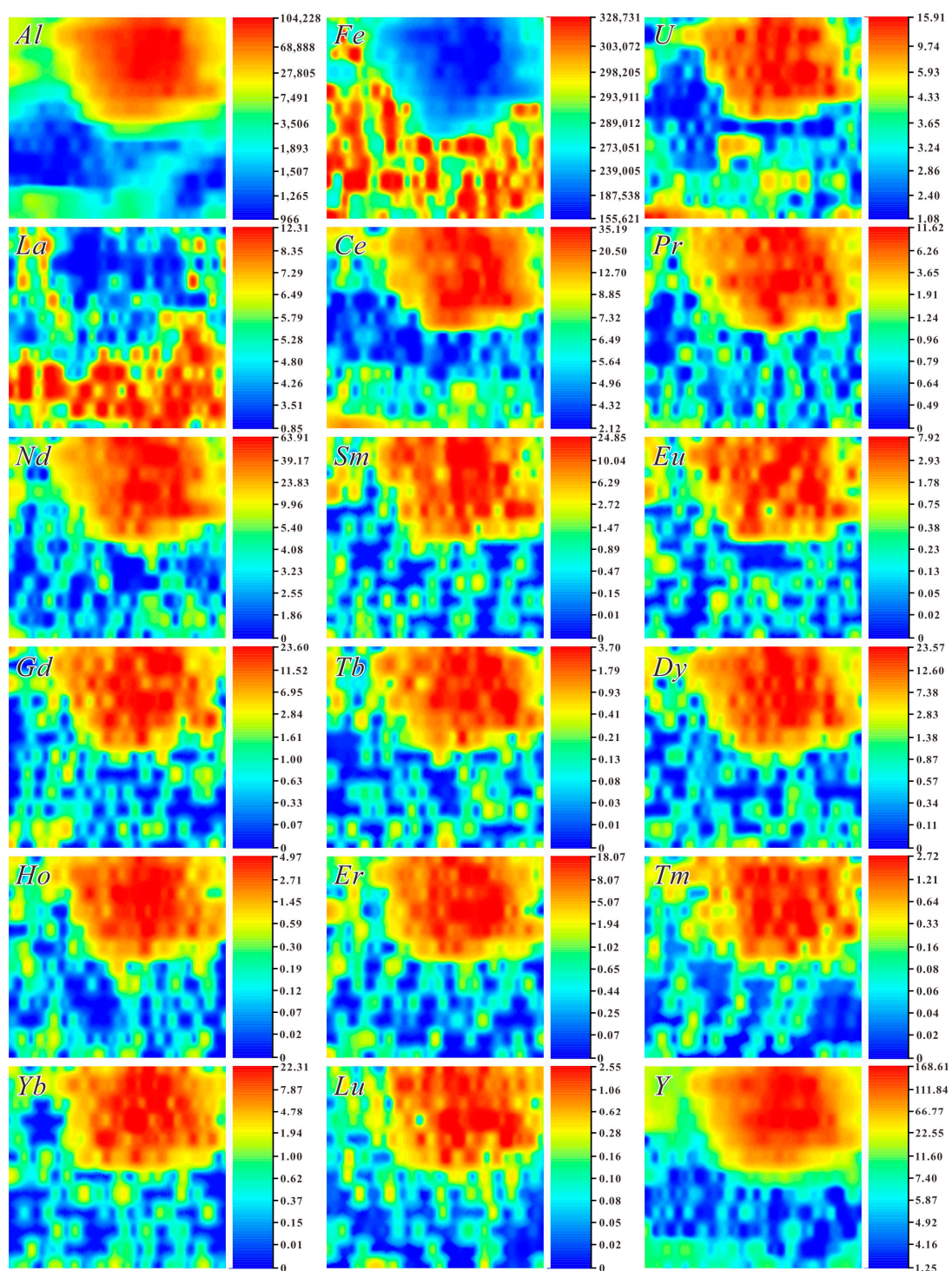
Figure 5. LA-ICP-MS trace element maps of the Xinqiao garnet; all maps show ppm abundances on a log scale.

5.2. U–Pb Dating

A total of 39 spot analyses for LA-ICP-MS U–Pb isotopic compositions were conducted on Sample XQ37-1, including 25 spots in Grt1 grains and 14 spots in Grt2 grains. U–Pb isotope data of the two-stage garnet are listed in Table 2.

Garnet commonly contains insignificant common Pb [23,24], and, thus, the Pb isotopic composition should be corrected prior to calculating ages. In this study, the ^{207}Pb-correction method was adopted [56,57]. The uncorrected data of Grt1 are plotted in the Tera–Wasserburg diagram (Figure 6a), and a regression through these analyses yields a lower-intercept age of 138 ± 16 Ma (MSWD = 1.5; N = 25) with an upper intercept value of 0.9975, which represents the initial ^{207}Pb/^{206}Pb [57] and can be used in an algorithm to allow a form of ^{207}Pb-correction [56]. Subsequently, the individual ^{207}Pb-corrected ^{206}Pb/^{238}U ages for Grt1 yield a weighted average age of 137.0 ± 7.8 Ma (MSWD = 4.9; Figure 6b). Similarly, the uncorrected data of Grt2 in the Tera–Wasserburg diagram (Figure 6c) yields a lower-intercept age of 131 ± 19 Ma (MSWD = 0.37; N = 14) with an upper intercept value of 0.9920, and the individual ^{207}Pb-corrected ^{206}Pb/^{238}U ages for Grt2 yield a weighted average age of 129.6 ± 7.1 Ma (MSWD = 1.6; Figure 6d).
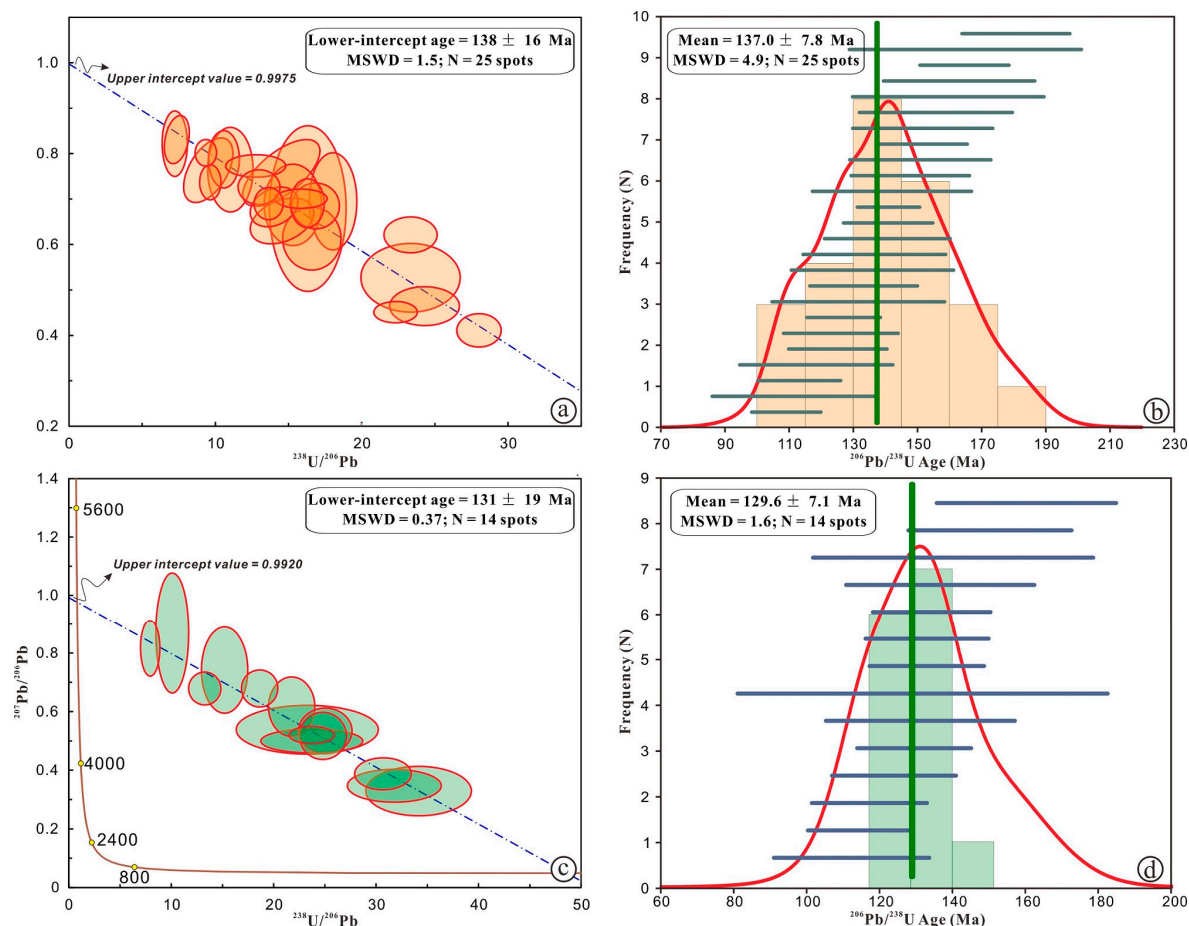

Figure 6. (**a**) Tera–Wasserburg diagram and (**b**) weighted average diagram of ^{207}Pb-corrected ^{206}Pb/^{238}U age for Grt1; (**c**) Tera–Wasserburg diagram and (**d**) weighted average diagram of ^{207}Pb-corrected ^{206}Pb/^{238}U age for Grt2.

Table 2. LA-ICP-MS U–Pb isotopic data of the Xinqiao garnets.

No.	Type	Pb (ppm)	^{204}Pb (ppm)	Th (ppm)	U (ppm)	Isotope Ratios							^{207}Pb-Based Age (Ma)	
						^{207}Pb/^{206}Pb	1sigma	^{207}Pb/^{235}U	1sigma	^{206}Pb/^{238}U	1sigma	rho	^{206}Pb/^{238}U	1sigma
1	Grt1	0.493	0.001	0.524	2.832	1.6060	0.3771	15.7253	1.5263	0.1386	0.0108	0.8025	162.6	11.9
2	Grt1	1.894	10.968	0.375	3.839	1.2654	0.1586	15.5996	1.1917	0.1360	0.0105	0.8432	151.3	11.0
3	Grt1	1.846	6.736	0.822	3.417	1.1679	0.1203	11.8480	0.6883	0.1071	0.0057	0.9090	140.4	7.1
4	Grt1	0.338	6.151	0.214	2.920	0.6358	0.1634	11.0720	1.1073	0.1051	0.0122	0.8365	164.6	18.2
5	Grt1	1.807	6.968	0.915	3.511	1.2147	0.1674	10.5318	0.6332	0.1035	0.0051	0.8229	180.4	8.5
6	Grt1	1.740	10.284	0.931	3.589	1.0366	0.1273	10.2757	0.8752	0.0945	0.0063	0.7845	132.8	8.5
7	Grt1	1.590	1.889	1.002	3.642	0.8259	0.0951	9.5730	1.1702	0.0907	0.0084	0.7536	141.6	12.5
8	Grt1	2.023	33.409	1.040	4.230	1.2031	0.3023	8.3650	0.9025	0.0784	0.0083	0.9809	118.0	12.0
9	Grt1	1.810	13.725	1.581	4.574	0.9962	0.1286	7.7180	0.6235	0.0770	0.0056	0.9047	140.2	9.9
10	Grt1	1.305	10.186	1.037	4.203	1.0495	0.1223	6.9929	0.4145	0.0734	0.0036	0.8167	151.2	7.1
11	Grt1	0.540	1.140	0.390	5.348	1.1069	0.2099	6.7314	0.5120	0.0714	0.0054	0.8103	150.5	11.1
12	Grt1	0.878	11.752	0.284	5.233	0.9875	0.1405	7.2062	0.6614	0.0689	0.0083	0.8246	111.1	12.9
13	Grt1	0.988	4.978	1.032	3.907	1.1379	0.2141	6.1846	0.5741	0.0687	0.0067	0.8580	159.2	15.0
14	Grt1	1.125	12.585	0.843	3.625	1.2107	0.2663	6.2044	0.7496	0.0654	0.0056	0.7035	136.2	11.2
15	Grt1	0.178	0.001	1.439	4.431	0.6198	0.1430	6.1056	0.4682	0.0631	0.0047	0.9656	125.7	9.0
16	Grt1	1.573	17.494	1.641	5.311	0.9616	0.0929	5.8652	0.4075	0.0615	0.0029	0.6804	126.6	5.8
17	Grt1	0.737	4.164	1.881	6.851	0.7704	0.1271	5.7500	1.1872	0.0613	0.0065	0.5160	131.1	13.6
18	Grt1	1.096	8.490	0.488	7.647	0.6550	0.0733	5.1011	0.5568	0.0603	0.0048	0.7296	155.4	12.0
19	Grt1	0.610	9.061	0.572	5.485	1.1300	0.2175	5.6147	0.4517	0.0594	0.0038	0.7962	124.7	7.8
20	Grt1	0.235	0.001	6.925	6.259	0.9177	0.3245	5.3206	0.6277	0.0554	0.0033	0.5058	112.7	6.5
21	Grt1	2.093	15.639	0.939	13.928	0.5873	0.0550	2.7959	0.1549	0.0449	0.0020	0.7896	164.3	7.0
22	Grt1	1.551	18.505	0.747	10.075	0.6754	0.1203	3.1180	0.4200	0.0429	0.0041	0.7129	135.5	12.7
23	Grt1	0.603	0.001	1.095	5.204	0.8704	0.1063	3.6740	0.2442	0.0429	0.0022	0.7758	108.6	5.5
24	Grt1	0.404	6.946	0.764	5.224	0.7346	0.1142	2.6421	0.2346	0.0412	0.0027	0.7252	147.4	9.3
25	Grt1	1.965	16.677	1.050	6.878	0.5219	0.0613	2.0284	0.1384	0.0357	0.0013	0.5246	140.6	4.9
38	Grt2	0.119	2.034	0.059	11.197	0.7552	0.1453	14.1736	1.5552	0.1255	0.0098	0.7113	112.9	10.7
39	Grt2	0.068	1.673	0.037	10.906	1.4342	0.5034	11.8783	2.2336	0.0989	0.0103	0.5564	115.2	7.1
40	Grt2	0.085	0.001	0.191	10.154	0.9470	0.0001	7.0769	0.6785	0.0754	0.0059	0.8221	117.9	7.9
41	Grt2	0.163	5.492	0.470	3.583	0.3452	0.0627	6.7435	1.1027	0.0658	0.0064	0.5968	124.6	8.5
42	Grt2	0.156	1.030	0.035	4.458	0.8896	0.2493	5.0365	0.4441	0.0537	0.0034	0.7177	130.1	7.8
43	Grt2	0.232	4.699	0.096	4.914	0.3830	0.0778	3.9199	0.5038	0.0460	0.0032	0.5339	131.7	12.9
44	Grt2	0.863	20.123	1.493	7.510	0.6869	0.1704	3.1965	0.7070	0.0429	0.0084	0.8868	132.5	25.4
45	Grt2	0.386	0.001	0.132	7.145	0.6542	0.0769	3.0401	0.2172	0.0422	0.0026	0.8565	133.6	7.9
46	Grt2	0.712	4.035	1.471	10.371	0.6087	0.1012	2.9120	0.4311	0.0421	0.0058	0.9335	133.7	8.5
47	Grt2	0.210	1.711	0.097	6.588	0.5874	0.1442	2.8859	0.3456	0.0403	0.0025	0.5125	135.0	8.1
48	Grt2	0.207	0.435	0.240	6.725	0.8929	0.1710	2.9508	0.3487	0.0400	0.0028	0.5894	137.5	12.8
49	Grt2	0.218	0.001	1.212	9.396	0.6567	0.1232	1.7524	0.1939	0.0326	0.0020	0.5411	140.9	19.1
50	Grt2	0.188	0.001	1.100	8.255	0.6584	0.1788	1.5127	0.2153	0.0315	0.0030	0.6664	151.2	11.1
51	Grt2	0.255	0.001	3.766	12.896	0.3070	0.0832	1.3361	0.2612	0.0293	0.0029	0.5083	160.9	12.2

6. Discussion

6.1. Occurrence of Uranium in the Garnet

Previous studies concluded that uranium primarily occurs as U-rich mineral inclusions in garnet, thus limiting the application of garnet U–Pb dating [58,59]. However, a relatively homogeneous distribution of U has been discovered in grandite from Nanminghe and Qicun iron skarn deposits in the North China Craton [22], indicating that U with high enough content for U–Pb dating can be hosted within the garnet structure. In this study, we found minor wollastonite, calcite, and quartz inclusions (Figures 4h,i), rather than U-rich mineral inclusions (monazite, zircon, titanite, and so on), in the grandite. LA-ICP-MS trace element mapping reveals not only the homogeneous U in Grt1 and locally enriched U in Grt2, but also the absence of chemical oscillatory zoning within Grt1 and Grt2 and the lack of mineral inclusions within Grt1. More importantly, the time-resolved signals of U, Al, Fe, Ca, Si, Ti, Y, and rare-earth elements (REEs), obtained by depth profile analyses of the observed two-stage garnets, are flat and stable (Figure 7), indicating the homogeneous distributions of these elements and possible absence of the U-rich mineral inclusions in grandite. This further suggests that U possibly occurs within the grandite structure.
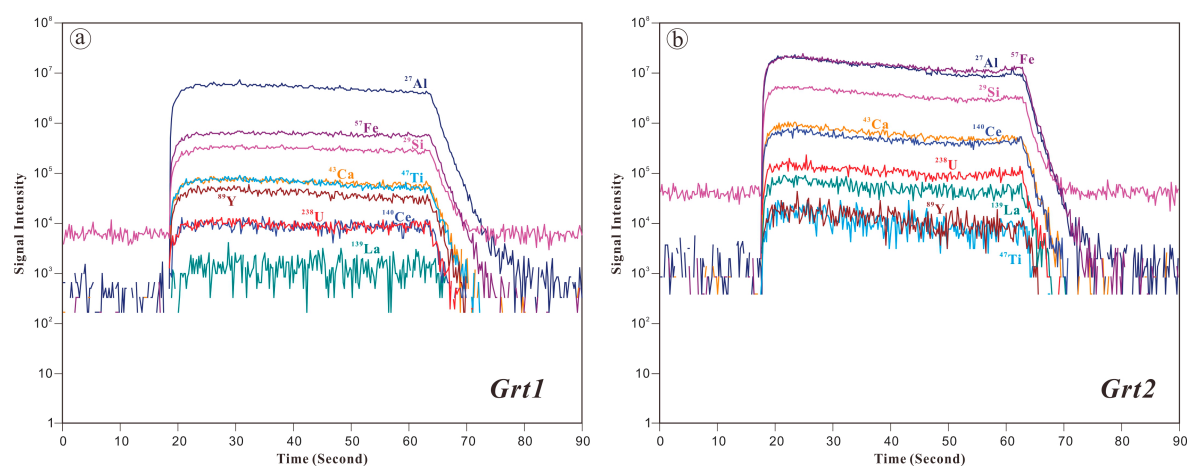

Figure 7. Representative time-resolved signals obtained by depth profile analyses of Grt1 (**a**) and Grt2 (**b**) from XQ37-1, showing flat and stable signals during laser ablation.

The radius of U^{4+} is similar to those of heavy rare earth element (HREE), commonly found in an eight-fold coordination site within the garnet, and, thus, U and HREE contents within garnet commonly show a positive correlation [60]. However, this positive correlation was not observed in the Xinqiao garnet (Figure 8a), indicating that the incorporation of U was not dominated by substitution mechanisms in the eight-fold coordination. On the other hand, the poor correlation between U and HREE also indicates that the primary U incorporation mechanism for the Xinqiao garnet is not surface sorption during rapid crystal growth of the garnet related to fluid infiltration, because surface sorption commonly causes U to correlate positively with both light rare earth element (LREE) and HREE in garnet [16,21]. For grandite or andradite, the incorporation of U is primarily achieved by coupled substitution of Ca^{2+} in the dodecahedral position on the basis of similar ionic radii and charge balance ($[U^{4+}]^{VIII} + 2[Fe^{3+}, Al^{3+}]^{IV} - [Ca^{2+}]^{VIII} + 2[Si^{4+}]^{IV}$) [11,16,60,61], which can be interpreted to be the U incorporation mechanism for the Xinqiao garnet. Uranium in both Grt1 and Grt2 has an obviously positive correlation with LREE (Figure 8b), especially La (Figure 8c), Ce (Figure 8d), Pr (Figure 8e), and Nd (Figure 8f), implying a similar substitution mechanism for LREEs in the Xinqiao garnet. Additionally, previous studies have documented that garnet has the distinct ability to fractionate REEs [11], which is evidenced in the Xinqiao garnet [18]. The positive correlation between U and LREEs (Figure 8b–f) further indicates that U is hosted within the garnet structure.
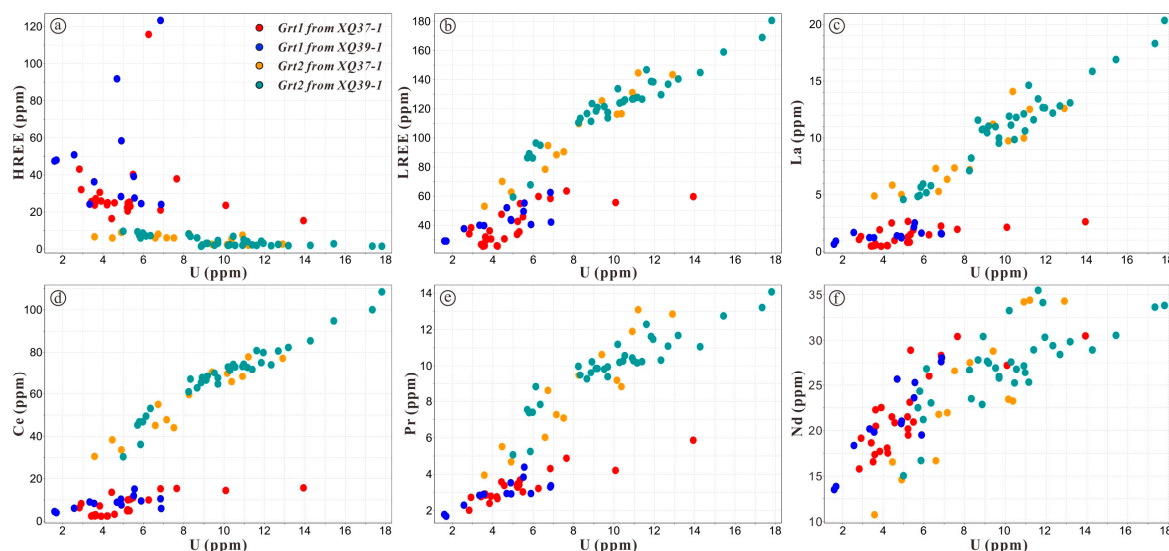
Figure 8. Correlation diagrams between U and (**a**) HREE contents, (**b**) LREE contents, (**c**) La contents, (**d**) Ce contents, (**e**) Pr contents and (**f**) Nd contents.

6.2. Timing of the Garnets and Mineralization

In this study, garnet U–Pb dating of Grt1 and Grt2 yielded weighted average $^{206}Pb/^{238}U$ ages of 137.0 ± 7.8 Ma and 129.6 ± 7.1 Ma, respectively. These two ages are similar within uncertainty, indicating that the timing between Grt1 and Grt2 was relatively short, and also close to the zircon U–Pb age (139.6 ± 1.5 Ma; [50]) of the Jitou stock, the pyrite Re–Os isochron age (126 ± 11 Ma; [62]) of the stratiform orebody, and the quartz fluid inclusion Rb–Sr isotope isochron age (138.0 ± 2.3 Ma, [50]) of the footwall stockwork mineralization. Although the Re–Os isochron age (319 ± 13 Ma; [39]) of pyrite from the footwall stockwork mineralization may imply Late Paleozoic submarine exhalative origin for the Xinqiao deposit, the initial value of $^{187}Os/^{188}Os$ (0.017) is inconsistent with the initial $^{187}Os/^{188}Os$ (1–8; [63]) of typical sedimentary exhalative deposit (SEDEX) deposits. Furthermore, the ^{187}Os and ^{187}Re contents in pyrites vary in a fairly narrow range, which does not meet the conditions of Re–Os isochron age; thus, this Re–Os isochron age is most likely not the true age of the footwall stockwork mineralization [64]. The combined geochronology shows that the stratiform mineralization formed in the Early Cretaceous (ca. 138 Ma), consistent with the primary formation age range (144–135 Ma; [65]) of porphyry–skarn Cu–Fe–Au–Mo deposits in the Middle–Lower Yangtze River Valley metallogenic belt and the Jurassic–Cretaceous tectono-thermal event in Eastern China [34].

6.3. Origin of the Garnet

As mentioned above, garnet can form via magmatic hydrothermal replacement, magmatism, and submarine sedimentary exhalative processes [2,40–42]. The two-stage garnet stages have weighted average $^{206}Pb/^{238}U$ ages of 137.0 ± 7.8 Ma and 129.6 ± 7.1 Ma, respectively, indicating that they are not linked to the late Paleozoic submarine exhalative processes. Moreover, garnet originating from submarine sedimentary exhalation is commonly almandine- and/or spessartine-rich due to the abundance of Mn and Fe on the seafloor [66,67]. The Xinqiao garnets were formed from grossular-andradite solid solution with low MnO (0.19–0.89%; [18]). Melt and fluid-melt inclusions are suggested to be a direct indicator for magmatic garnets [68–70], yet they were not found in the garnets from the stratiform orebody [71]. Moreover, magmatic processes are not expected to significantly fractionate Y from Ho [72]; hence, magmatic garnets would have Y/Ho close to the chondrite value of 28 [73]. Grt1 and Grt2, however, have Y/Ho ratios ranging from 36.9 to 47.8 (38.6–47.8 for Grt1 from XQ37-1; 36.9–45.8 for Grt1 from XQ39-1) and 31.5 to 60.0 (36.4–60.0 for Grt2 from XQ37-1; 31.5–53.3 for Grt2 from XQ39-1), respectively. Previous studies on the Xinqiao stratiform orebody, including the H–O isotope data obtained from the ore-bearing quartz, reveal the magmatic hydrothermal characteristics of the ore-forming fluid [74]. Iron isotope compositions of pyrites from Xinqiao ($\delta^{57}Fe$

ranges from −1.22‰ to 0.15‰; [75]) are similar to the pyrites in the skarn system (δ^{57}Fe ranges from −2.58‰ to 1.62‰; [76]), and the initial ^{87}Sr/^{86}Sr value (0.71138 ± 0.00014; [50]) of the footwall stockwork mineralization is close to that of the Jitou stock. All this evidence indicates that the stratiform orebody may have been associated with the magmatic hydrothermal fluids derived from the Jitou stock, and generated by the Early Cretaceous tectono-thermal event in Eastern China. Therefore, we infer that the garnet hosted in the stratiform orebody is likely to be of magmatic hydrothermal replacement origin, associated with the Jitou stock, as confirmed by the similar ages of garnet and magmatism.

7. Conclusions

The major findings of this study can be summarized as follows:

(1) Garnets from the Xinqiao stratiform orebody can be divided into early garnet (Grt1) and late garnet (Grt2) generations. Grt1 and Grt2 yielded weighted average ^{207}Pb-correction ^{206}Pb/^{238}U ages of 137.0 ± 7.8 Ma (MSWD = 4.9) and 129.6 ± 7.1 Ma (MSWD = 1.6), respectively, close to the zircon U–Pb age of the Jitou stock, indicating that they formed in the Early Cretaceous.

(2) The Xinqiao garnet and stratiform mineralization may have formed from Early Cretaceous magmatic–hydrothermal fluids associated with the Jitou stock, and were generated by the Early Cretaceous tectono-thermal event in Eastern China.

Author Contributions: Yu Zhang, Yongjun Shao and Huayong Chen conceived and designed the experiments; Rongqing Zhang and Dengfeng Li performed the experiments; Zhongfa Liu analyzed the data; Yu Zhang, Huayong Chen and Dengfeng Li wrote the paper.

Conflicts of Interest: The authors declare no conflict of interest.

References

1. Meinert, L.D. Skarns and skarn deposits. *Geosci. Can.* **1992**, *19*, 145–162.
2. Meinert, L.D.; Dipple, G.M.; Nicolescu, S. World Skarn Deposits. In *Economic Geology 100th Anniversary Volume 1905–2005*; Elsevier: Amsterdam, The Netherlands, 2005; pp. 299–336.
3. Porter, S.J.; Selby, D. Rhenium–Osmium (Re–Os) molybdenite systematics and geochronology of the Cruachan Granite skarn mineralization, Etive Complex: Implications for emplacement chronology. *Scott. J. Geol.* **2010**, *46*, 17–21.
4. Xia, R.; Wang, C.M.; Qing, M.; Deng, J.; Carranza, E.J.M.; Li, W.L.; Guo, X.D.; Ge, L.S.; Yu, W.Q. Molybdenite Re–Os, zircon U–Pb dating and Hf isotopic analysis of the Shuangqing Fe–Pb–Zn–Cu skarn deposit, East Kunlun Mountains, Qinghai Province, China. *Ore Geol. Riv.* **2015**, *66*, 114–131.
5. Li, J.W.; Deng, X.D.; Zhou, M.F.; Liu, Y.S.; Zhao, X.F.; Guo, J.L. Laser ablation ICP-MS titanite U–Th–Pb dating of hydrothermal ore deposits: A case study of the Tonglushan Cu–Fe–Au skarn deposit, SE Hubei Province, China. *Chem. Geol.* **2010**, *270*, 56–67.
6. Fu, Y.; Sun, X.M.; Zhou, H.Y.; Lin, H.; Yang, T.J. In-situ LA-ICP-MS U–Pb geochronology and trace elements analysis of polygenetic titanite from the giant Beiya gold–polymetallic deposit in Yunnan Province, Southwest China. *Ore Geol. Rev.* **2016**, *77*, 43–56.
7. Oyman, T. Geochemistry, mineralogy and genesis of the Ayazmant Fe–Cu skarn deposit in Ayvalik, (Balikesir), Turkey. *Ore Geol. Rev.* **2010**, *37*, 175–201.
8. Lieben, F.; Moritz, R.; Fontbote, L. Mineralogy, Geochemistry, and Age Constraints on the Zn–Pb Skarn Deposit of Maria Cristina, Quebrada Galena, Northern Chile. *Econ. Geol.* **2000**, *95*, 1185–1196.
9. Li, H.; Yonezu, K.; Watanabe, K.; Tindell, T. Fluid origin and migration of the Huangshaping W–Mo polymetallic deposit, South China: Geochemistry and ^{40}Ar/^{39}Ar geochronology of hydrothermal K-feldspars. *Ore Geol. Rev.* **2017**, *86*, 117–129.
10. Li, H.Q.; Xie, C.F.; Chang, H.L. *Geochronology of Mineralization of Nonferrous and Precious Metallic Deposits in Northern Xinjiang*; Geological Publishing House: Beijing, China, 1998; 264p. (In Chinese)

11. Gaspar, M.; Knaack, C.; Meinert, L.D.; Moretti, R. REE in skarn systems: A LA-ICP-MS study of garnets from the Crown Jewel gold deposit. *Geochim. Cosmochim. Acta* **2008**, *72*, 185–205.

12. Yardley, B.W.; Rochelle, C.A.; Barnicoat, A.C.; Lloyd, G.E. Oscillatory zoning in metamorphic minerals: An indicator of infiltration metasomatism. *Mineral. Mag.* **1991**, *55*, 357–365.

13. Jamtveit, B.; Wogelius, R.A.; Fraser, D.G. Zonation patterns of skarn garnets: Records of hydrothermal system evolution. *Geology* **1993**, *21*, 113–116.

14. Crowe, D.E.; Riciputi, L.R.; Bezenek, S.; Ignatiev, A. Oxygen isotope and trace element zoning in hydrothermal garnets: Windows into large-scale fluid flow behavior. *Geology* **2001**, *29*, 479–482.

15. Fernando, G.; Hauzenberger, C.A.; Baumgartner, L.P.; Hofmeister, W. Modeling of retrograde diffusion zoning in garnet: Evidence for slow cooling of granulites from the Highland Complex of Sri Lanka. *Mineral. Petrol.* **2003**, *78*, 53–71.

16. Smith, M.P.; Henderson, P.; Jeffries, T.E.R.; Long, J.; Williams, C.T. The rare earth elements and uranium in garnets from the Beinn and Dubhaich Aureole, Skye, Scotland, UK: Constraints on processes in a dynamic hydrothermal system. *J. Petrol.* **2004**, *45*, 457–484.

17. Martin, L.A.J.; Ballèvre, M.; Boulvais, P.; Halfpenny, A.; Vanderhaeghe, O.; Duchêne, S.; Deloule, E. Garnet re-equilibration by coupled dissolution-reprecipitation: Evidence from textural, major element and oxygen isotope zoning of 'cloudy' garnet. *J. Metamorph. Geology* **2011**, *29*, 21–231.

18. Zhang, Y.; Shao, Y.J.; Wu, C.D.; Chen, H.Y. LA-ICP-MS trace element geochemistry of garnets: Constraints on hydrothermal fluid evolution and genesis of the Xinqiao Cu–S–Fe–Au deposit, eastern China. *Ore Geol. Rev.* **2017**, *86*, 426–439.

19. Smit, M.A.; Scherer, E.E.; Mezger, K. Lu–Hf and Sm–Nd garnet geochronology: Chronometric closure and implications for dating petrological processes. *Earth Planet. Sci. Lett.* **2013**, *381*, 222–233.

20. Blichert-Toft, J. On the Lu–Hf isotope geochemistry of silicate rocks. *Geostand. Geoanal. Res.* **2001**, *25*, 41–56.

21. Jamtveit, B.; Hervig, R.L. Constraints on transport and kinetics in hydrothermal systems from zoned garnet crystals. *Science* **1994**, *263*, 505–508.

22. Deng, X.D.; Li, J.W.; Luo, T.; Wang, H.Q. Dating magmatic and hydrothermal processes using andradite-rich garnet U–Pb geochronometry. *Contrib. Mineral. Petrol.* **2017**, *172*, doi:10.1007/s00410-017-1389-2.

23. DeWolf, C.; Zeissler, C.J.; Halliday, A.; Mezger, K.; Essene, E. The role of inclusions in U–Pb and Sm–Nd garnet geochronology: Stepwise dissolution experiments and trace uranium mapping by fission track analysis. *Geochim. Cosmochim. Acta* **1996**, *60*, 121–134.

24. Yudintsev, S.V.; Lapina, M.I.; Ptashkin, A.G.; Ioudintseva, T.S.; Utsunomiya, S.; Wang, L.M.; Ewing, R.C. Accommodation of Uranium Into the Garnet structure. In *Proceedings of the Materials Research Society Symposium, San Francisco, CA, USA, 2–5 April 2002*; Cambridge University Press: Cambridge, UK, 2002; p. JJ11.

25. Seman, S.; Stockli, D.F.; McLean, N.M. U–Pb geochronology of grossular-andradite garnet. Chemical *Geology* **2017**, *460*, 106–116.

26. Mao, J.W.; Xie, G.Q.; Duan, C.; Franco, P.; Dazio, I.; Chen, Y.C. A tectono-genetic model for porphyry–skarn–stratabound Cu–Au–Fe and magnetite–apatite deposit along the Middle–Lower Yangtze river valley, Eastern China. *Ore Geol. Rev.* **2011**, *43*, 294–314.

27. Chang, Y.F.; Liu, X.P.; Wu, Y.Z. *Metallogenic Belt of the Middle–Lower Yangtze River*; Geological Publishing House: Beijing, China, 1991; 379p. (In Chinese)

28. Fu, S.G.; Yan, X.Y.; Yuan, C.X. Geologic feature of submarine volcanic eruption- sedimentary pyrite type deposit in Carboniferous in the Middle–Lower Yangtze River Valley metallogenic belt, Eastern China. *J. Nanjing Univ. Nat. Sci. Ed.* **1977**, *4*, 43–67. (In Chinese)

29. Gu, L.X.; Xu, K.Q. On the carboniferous submarine massive sulfide deposit in the lower reaches of the Yangtze River. *Acta Geol. Sin.* **1986**, *60*, 176–188. (In Chinese)

30. Gu, L.X.; Hu, W.X.; He, J.X. Regional variations in ore composition and fluid features of massive sulfide deposits in South China: Implications for genetic modeling. *Episodes* **2000**, *23*, 110–118.

31. Xu, W.Y.; Yang, Z.S.; Meng, Y.F.; Zeng, P.S.; Shi, D.N.; Tian, S.H.; Li, H.Y. Genetic Model and Dynamic Migration of Ore-forming Fluids in Carboniferous Exhalation-Sedimentary Massive Sulfide Deposits in Tongling District, Anhui Province. *Miner. Depos.* **2004**, *23*, 353–364. (In Chinese)

32. Chang, Y.F.; Liu, X.G. Layer control type skarn type deposit—some deposits in the Middle-Lower Yangtze Depression in Anhui Province as an example. *Miner. Depos.* **1983**, *2*, 11–20. (In Chinese)

33. Pan, Y.; Done, P. The lower Changjiang (Yangtzi/Yangtze River) metallogenic belt, east–center China: Intrusion and wall rock hosted Cu–Fe–Au, Mo, Zn, Pb, Ag deposits. *Ore. Geol. Rev.* **1999**, *15*, 177–242.

34. Mao, J.W.; Shao, Y.J.; Xie, G.Q.; Zhang, J.D.; Chen, Y.C. Mineral deposit model for porphyry–skarn polymetallic copper deposits in Tongling ore dense district of Middle-Lower Yangtze Valley metallogenic belt. *Miner. Depos.* **2009**, *28*, 109–119. (In Chinese)

35. Zhang, Y.; Shao, Y.J.; Chen, H.Y.; Liu, Z.F.; Li, D.F. A hydrothermal origin for the large Xinqiao Cu–S–Fe deposit, Eastern China: Evidence from sulfide geochemistry and sulfur isotopes. *Ore Geol. Rev.* **2017**, *88*, 534–549.

36. Yang, D.F.; Fu, D.X.; Wu, N.X. Genesis of pyrite type copper in Xinqiao and its neighboring region according to ore composition and structure. *Issue Nanjing Inst. Geol. Miner. Resour. Chin. Acad. Geol. Sci.* **1982**, *3*, 59–68. (In Chinese)

37. Xie, H.G.; Wang, W.B.; Li, W.D. The genesis and metallogenetic of Xinqiao Cu–S–Fe deposit, Anhui Province. *Volcanol. Miner. Resour.* **1995**, *16*, 101–107. (In Chinese)

38. Zhou, T.F.; Zhang, L.J.; Yuan, F.; Fang, Y.; Cooke, D.R. LA-ICP-MS in situ trace element analysis of pyrite from the Xinqiao Cu–Au–S Deposit in Tongling, Anhui, and its constrains on the ore genesis. *Earth Sci. Front.* **2010**, *17*, 306–319. (In Chinese)

39. Guo, W.M.; Lu, J.J.; Jiang, S.Y.; Zhang, R.Q.; Qi, L. Re–Os isotope dating of pyrite from the footwall mineralization zone of the Xinqiao deposit, Tongling, Anhui Province: Geochronological evidence for submarine exhalative sedimentation. *Chin. Sci. Bull.* **2011**, *56*, 3860–3865. (In Chinese)

40. Einaudi, M.T.; Burt, D.M. Introduction-terminology, classification, and composition of skarn deposits. *Econ. Geol.* **1982**, *77*, 745–754.

41. Doyle, M.G.; Allen, R.L. Subseafloor replacement in volcanic-hosted massive sulfide deposits. *Ore Geol. Rev.* **2003**, *23*, 183–222.

42. Zhang, Y.; Shao, Y.J.; Chen, H.Y.; Liu, Z.F.; Li, D.F. Fingerprinting the hydrothermal fluid characteristics from LA-ICP-MS Ttrace element geochemistry of garnet in the Yongping Cu deposit, SE China. *Minerals* **2017**, *7*, 199.

43. Xu, G.; Zhou, J. The Xinqiao Cu–S–Fe–Au deposit in the Tongling mineral district, China: Synorogenetic remobilization of a stratiform sulfide deposit. *Ore Geol. Rev.* **2001**, *18*, 77–94.

44. Tang, Y.C.; Wu, Y.Z.; Cu, G.Z.; Xing, F.M.; Wang, Y.M.; Cao, F.Y.; Chang, Y.F. *Copper Gold Polymetallic Ore Deposit Geology in the Region along Yangtze River in Anhui Province*; Geological Publishing House: Beijing, China, 1998; 351p. (In Chinese)

45. Wu, C.L.; Dong, S.W.; Robinson, P.T.; Frost, B.R.; Gao, Y.H.; Lei, M.; Chen, Q.L.; Qin, H.P. Petrogenesis of high-K, calc-alkaline and shoshonitic intrusive rocks in the Tongling area, Anhui Province (eastern China), and their tectonic implications. *Geol. Soc. Am. Bull.* **2014**, *126*, 78–102.

46. Zhai, Y.S.; Yao, S.Z.; Lin, X.D.; Jin, F.Q.; Zhou, X.R.; Wan, T.F.; Zhou, Z.G. Metallogenic regularity of iron and copper deposits in the Middle–Lower valley of the Yangtze River. *Miner. Depos.* **1992**, *11*, 1–235. (In Chinese)

47. Cao, Y.; Zheng, Z.J.; Du, Y.L.; Gao, F.P.; Qin, X.L.; Yang, H.M.; Lu, Y.H.; Du, Y.S. Ore geology and fluid inclusions of the Hucunnan deposit, Tongling, Eastern China: Implications for the separation of copper and molybdenum in skarn deposits. *Ore Geol. Rev.* **2017**, *81*, 925–939.

48. Du, Y.L.; Deng, J.; Cao, Y.; Li, D.D. Petrology and geochemistry of Silurian–Triassic sedimentary rocks in the Tongling region of Eastern China: Their roles in the genesis of large stratabound skarn ore deposits. *Ore Geol. Rev.* **2015**, *67*, 255–263.

49. Wang, S.W.; Zhou, T.F.; Yuan, F.; Fan, Y.; Zhang, L.J.; Song, Y.L. Petrogenesis of Dongguashan skarn–porphyry Cu–Au deposit related intrusion in the Tongling district, eastern China: Geochronological, mineralogical, geochemical and Hf isotopic evidence. *Ore Geol. Rev.* **2015**, *64*, 53–70.

50. Zhang, Y.; Shao, Y.J.; Li, H.B.; Liu, Z.F. Genesis of the Xinqiao Cu–S–Fe–Au deposit in the Middle–Lower Yangtze River Valley metallogenic belt, Eastern China: Constraints from U–Pb–Hf, Rb–Sr, S, and Pb isotopes. *Ore Geol. Rev.* **2017**, *86*, 100–116.

51. Zang, W.S.; Wu, G.G.; Zhang, D.; Liu, A.H. Geological and geochemical characteristics and genetic analyses of Xinqiao Iron Orefield, Tongling. *Geotecton. Metallog.* **2004**, *28*, 187–193. (In Chinese)

52. Wang, Y.; Zhu, X.L.; Mao, J.W.; Li, Z.H.; Cheng, Y.B. Iron isotope fractionation during skarn-type metallogeny: A case study of Xinqiao Cu–S–Fe–Au Deposit in the Middle–Lower Yangtze Valley. *Ore Geol. Rev.* **2011**, *43*, 194–202.

53. Zhai, D.G.; Liu, J.J.; Zhang, H.Y.; Wang, J.P.; Su, L.; Yang, X.A.; Wu, S.H. Origin of oscillatory zoned garnets from the Xieertala Fe–Zn skarn deposit, northern China: In situ LA-ICP-MS evidence. *Lithos* **2014**, 190–191, 279–291.

54. Liu, Y.S.; Gao, S.; Hu, Z.C.; Gao, C.G.; Zong, K.Q.; Wang, D.B. Continental and oceanic crust recycling-induced melt-peridotite interactions in the Trans-North China Orogen: U–Pb dating, Hf isotopes and trace elements in zircons of mantle xenoliths. *J. Petrol.* **2010**, *51*, 537–571.

55. Ludwig, K.R. *Use's Manual for Isoplot 3.0: A Geochronological Toolkit for Microsoft Excel*; Special Publication, 4; Berkeley Geochronology Center: Berkeley, CA, USA, 2003; 70p.

56. Stern, R.A. The GSC sensitive high resolution ion microprobe (SHRIMP): Analytical techniques of zircon U–Th–Pb age determinations and performance evaluation. Radiogenic age and isotopic studies: Report 10. *Geol. Surv. Can. Curr. Res.* **1997**, *1997-F*, 1–31.

57. Aleinikoff, J.N.; Wintsch, R.P.; Fanning, C.M.; Dorais, M.J. U–Pb geochronology of zircon and polygenetic titanite from the Glastonbury Complex, Connecticut, USA: An integrated SEM, EMPA, TIMS, and SHRIMP study. *Chem. Geol.* **2002**, *188*, 125–147.

58. Vance, D.; Meier, M.; Oberli, F. The infuence of high U–Th inclusions on the U–Th–Pb systematics of almandine-pyrope garnet: Results of a combined bulk dissolution, stepwise-leaching, and SEM study. *Geochim. Cosmochim. Acta* **1998**, *62*, 3527–3540.

59. Lima, S.M.; Corfu, F.; Neiva, A.M.R.; Ramos, J.M.F. U–Pb IDTIMS dating applied to U-rich inclusions in garnet. *Am. Mineral.* **2012**, *97*, 800–806.

60. Shannon, R.D. Revised effective ionic radii and systematic studies of interatomic distances in halides and chalcogenides. *Acta Crystallogr. Sect. A* **1976**, *32*, 751–767.

61. Dziggel, A.; Wulff, K.; Kolb, J.; Meyer, F.M.; Lahaye, Y. Oscillatory zoning in metamorphic minerals: An indicator of infiltration metasomatism. *Chem. Geol.* **2009**, *262*, 262–276.

62. Xie, J.C.; Yang, X.Y.; Du, J.G.; Du, X.W.; Xiao, Y.L.; Qu, W.J.; Sun, W.D. Re–Os precise dating of pyrite from the Xinqiao Cu–Au–Fe–S Deposit in Tongling, Anhui and its implications for mineralization. *Geol. Sci.* **2009**, *44*, 183–192. (In Chinese)

63. Ravizza, G.; Martin, C.E.; German, C.R.; Thompson, G. Os isotopes as tracers in seafloor hydrothermal system: Metalliferous deposits from the TAG hydrothermal area, 26° N Mid-Atlantic Ridge. *Earth Plant. Sci. Lett.* **1996**, *138*, 105–119.

64. Huang, G.H. Mineralization Characteristics and Genesis of Xinqiao Cu–S–Au Polymetallic Deposit, Tongling, Anhui Province, China. Master's Thesis, China University of Geosciences, Wuhan, China, 2011. (In Chinese)

65. Mao, J.W.; Wang, Y.T.; Lehmann, B.; Du, A.D.; Mei, Y.X.; Li, Y.F.; Zang, W.S.; Stein, H.J.; Zhou, T.F. Molybdenite Re–Os and albite ^{40}Ar–^{39}Ar dating of Cu–Au–Mo and magnetite systems in the Yangtze River valley and metallogenic implications. *Ore Geol. Rev.* **2006**, *29*, 307–324.

66. Gemmell, J.B.; Zantop, H.; Meinert, L.D. Genesis of the Aguilar zinc-lead-silver deposit, Argentina; contact metasomatic vs. sedimentary exhalative. *Econ. Geol.* **1992**, *87*, 2085–2112.

67. Burton, K.W.; Bourdon, B.; Birck, J.L.; Allègre, C.J.; Hein, J.R. Osmium isotope variations in the oceans recorded by Fe–Mn crusts. *Earth Planet. Sci. Lett.* **1999**, *171*, 185–197.

68. Ling, Q.C.; Cheng, H.L. Discussion on forming process and geological characteristics of magmatic skarn in Tongling area, Anhui Province. *J. Changchun Univ. Sci. Technol.* **1998**, *28*, 366–371. (In Chinese)

69. Xiao, C.D.; Liu, X.W. REE geochemistry and origin of skarn garnets from eastern Inner Mongolia. *Geol. China* **2002**, *29*, 311–316. (In Chinese)

70. Zheng, Z.; Du, Y.S.; Cao, Y.; Cao, Z.W.; Yang, S.; Dong, Q. The composition characteristics and origin of garnets in the Dongguashan skarn copper deposit, Anhui Province, China. *Acta Petrol. Mineral.* **2012**, *31*, 235–242. (In Chinese)

71. Zhang, Y. Genesis of Xinqiao Cu–S–Fe deposit, Tongling, Anhui Province, China. Ph.D. Thesis, Central South University, Changsha, China, 2015; 157p. (In Chinese)

72. Bau, M.; Dulski, P. Anthropogenic origin of positive gadolinium anomalies in river waters. *Earth Planet. Sci. Lett.* **1996**, *143*, 245–255.

73. Anders, M.; Grevesse, N. Abundances of the elements: Meteoritic and solar. *Geochim. Cosmochim. Acta* **1989**, *53*, 197–214.

74. Liu, X.B. Geological characteristics and ore-controlling factor analysis of Xinqiao S–Fe deposit. *Express Inf. Min. Ind.* **2002**, *19*, 13–15. (In Chinese)

75.   Wang, Y.; Zhu, X.K.; Cheng, Y.B. Ore microscopy & Fe isotope of the Xinqiao deposit and their constraints on the ore genesis. *J. Jilin Univ. Earth Sci. Ed.* **2013**, *43*, 1787–1798. (In Chinese)

76.   Graham, S.; Pearson, N.; Jackson, S.; Griffin, W.; O'Reilly, S.Y. Tracing Cu and Fe from source to porphyry: In situ determination of Cu and Fe isotope ratios in sulfides from the Grasberg Cu–Au deposit. *Chem. Geol.* **2004**, *207*, 147–169.